Journal of Materials Chemistry A

ROYAL SOCIETY OF CHEMISTRY

COMMUNICATION

View Article Online
View Journal | View Issue

Check for updates

Cite this: J. Mater. Chem. A, 2023, 11, 12719

Received 20th April 2023
Accepted 9th May 2023

DOI: 10.1039/d3ta02348f

rsc.li/materials-a

Published on 12 Motsheanong 2023. Downloaded on 2025-09-05 03:40:57.

Enhanced photocatalytic hydrogen production of microporous organic polymers by incorporation of afterglow phosphorescent materials†

Sang Hyun Ryu, [a] Gye Hong Kim, [b] Tae Kyu Ahn, *[ac] Kyoung Chul Ko *[d] and Seung Uk Son *[a]

This work shows that photocatalytic hydrogen evolution from water by microporous organic polymer (MOP)-based photocatalysts can be enhanced by the incorporation of afterglow phosphorescent materials (AG). The photocatalytic MOPs were introduced on the surface of AG through the Stille coupling of tris(4-trimethylstannylphenyl)amine with 3,7-dibromodibenzothiophene sulfone. The resultant AG–MOP–TADS–Pds showed enhanced photocatalytic activities by 2.4 times, compared with MOP–TADS–Pd, due to the Förster resonance energy transfer or charge transfer between AG and MOP–TADS–Pds.

10th anniversary statement

We congratulate the Royal Society of Chemistry on the last 10 years of success of the *Journal of Materials Chemistry A*. It was our pleasure to see the surprising growth of the *Journal of Materials Chemistry A*. We have studied morphology-engineered microporous organic polymers (ME-MOPs) as functional materials for environmental and energy issues. Fortunately, we found that our research theme fits well with the *Journal of Materials Chemistry A*. We have enjoyed the rapid and convenient reviewing and publication process. As the reputation and criteria of the *Journal of Materials Chemistry A* grew, we could follow and improve the quality of our research. We hope for the continued success of the *Journal of Materials Chemistry A* and appreciate the efforts of editorial offices and reviewers. It will be our honor to submit our future works to the *Journal of Materials Chemistry A*.

As global climate changes triggered by the consumption of fossil fuels come to pose actual threats to human life, carbon neutralization is becoming an increasingly important subject.[1] In this regard, hydrogen has continually attracted attention as an alternative fuel instead of petroleum.[2] To realize the hydrogen economy, the technologies of hydrogen generation, storage, and utilization must first be sufficiently accumulated and revolutionized.[2]

Photocatalytic water splitting is one of the promising methods for the generation of hydrogen.[3] Over the last several decades, various photocatalytic systems have been developed for water splitting.[4] Moreover, there has recently been great progress in microporous organic polymer (MOP)-based photocatalytic systems for the generation of hydrogen from water.[5–8] MOPs can be prepared by the coupling of organic building blocks.[9] Due to the network feature of MOPs, MOP-based photocatalytic systems showed enhanced stability in photocatalytic hydrogen production, compared with molecule-based photocatalysts.[10] The introduction of electron push–pull structures into MOP-based photocatalysts can induce efficient utilization of visible light, thus resulting in enhanced photocatalytic performance.[10] Further, residual palladium nanoparticles play critical roles as catalysts in the efficient photocatalytic production of hydrogen.[11] However, new approaches should be continuously explored to enhance the photocatalytic performance of MOP-based photocatalysts.

While the performance of photocatalysts is highly important, efficient utilization of light is also a crucial point to consider. In this regard, collecting and concentrating light has been studied as a strategy to enhance the performance of light-related systems such as solar cells.[12] We have shown that afterglow phosphorescent materials are helpful for the utilization of light by MOP-based photocatalysts. Afterglow phosphorescent materials have been utilized for emergency notifications in dark surroundings (Fig. 1a).[13] When afterglow phosphorescent materials absorb light, they gradually emit visible light.[13] One of the commercial afterglow phosphorescent materials is $Sr_4Al_{14}O_{25}$ with doped Eu, Dy, and B (denoted by AG).[14] After

[a]Department of Chemistry, Sungkyunkwan University, Suwon 16419, Korea. E-mail: sson@skku.edu

[b]Department of Earth Systems and Environmental Sciences, Chonnam National University, Gwangju 61186, Korea

[c]Department of Energy Science, Sungkyunkwan University, Suwon 16419, Korea. E-mail: taeahn@skku.edu

[d]Department of Chemistry Education, Chonnam National University, Gwangju 61186, Korea. E-mail: kcho1982@jnu.ac.kr

† Electronic supplementary information (ESI) available: Experimental procedures, computational simulation, additional characterization data, and comparative photocatalytic performance of MOP-based photocatalysts. See DOI: https://doi.org/10.1039/d3ta02348f

Published on 12 Motsheanong 2023. Downloaded on 2025-09-05 03:40:57.

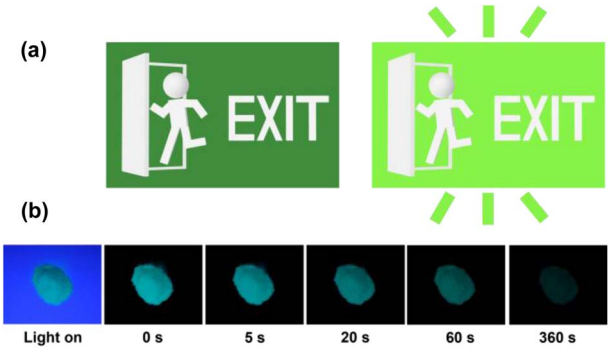

Fig. 1 (a) An example of the application of afterglow phosphorescent materials in common life. (b) Afterglow properties of commercial $Sr_4Al_{14}O_{25}$:Eu,Dy,B used in this study.

exposure to light, the commercial AG used in this study could maintain emission for ~6 minutes (Fig. 1b).

Our research group has reported that the morphology control of MOPs can enhance their functional performance.[15] For example, the nanorods and hollow spheres of photocatalytic MOPs have shown enhanced photocatalytic performance in hydrogen production from water.[10,16] We have also shown that the MOPs can be incorporated into various inorganic materials including metal oxides.[17] Here, we expect that incorporating photocatalytic MOPs into AG can enhance their photocatalytic performance, due to the additional utilization of light. In this work, we report the synthesis of AG–MOP composites and their enhanced photocatalytic performance.

Fig. 2 shows the synthetic method used for the composites (AG–MOP–TADS–Pds) of AG, MOP bearing triphenylamines and dibenzothiophene sulfones, and Pd in addition to the control materials (AG–Pd, MOP–TADS–Pd2). In the presence of commercial AG ($Sr_4Al_{14}O_{25}$:Eu,Dy,B), the Stille coupling of tris(4-trimethylstannylphenyl)amine with 1.5 eq. of 3,7-dibromodibenzothiophene sulfone by a $(PPh_3)_4Pd$ catalyst resulted in the formation of AG–MOP–TADS–Pds. The amounts of organic building blocks were carefully optimized to suppress the independent formation of MOP–TADS–Pds. With a fixed amount of AG (60 mg), the amounts of organic building blocks were gradually reduced. When 27 μmol of tris(4-trimethylstannylphenyl)amine and 40 μmol of 3,7-dibromodibenzothiophene sulfone were used, the independent formation of MOP–TADS–Pds was significantly suppressed.

It has been reported that the optimal amount of Pd is critical for achieving high performance MOP-based photocatalysts for water splitting.[16] If the amount of Pd is insufficient, the catalytic performance is reduced, due to the less efficient redox reaction on the Pd. If the amount of Pd is excessive, it can hinder the light harvesting of MOP materials (Fig. S1 in the ESI†). In this regard, we varied the amount of $(PPh_3)_4Pd$ from 11 μmol to 32 and 64 μmol with optimal amounts of organic building blocks to form three AG–MOP–TADS–Pds, which were denoted as AG–MOP–TADS–Pd1–3, respectively. As a control material, AG–Pd was prepared by the treatment of AG under the same synthetic conditions as AG–MOP–TADS–Pd2 without using organic

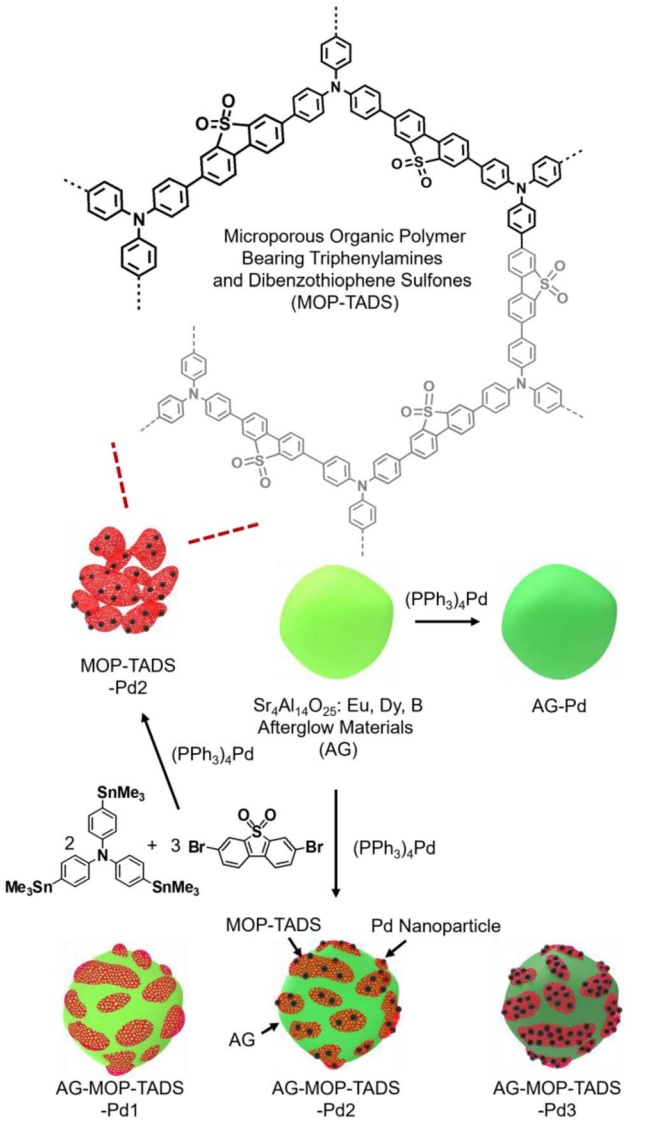

Fig. 2 Synthesis of the composites (AG–MOP–TADS–Pds) of AG, MOP bearing triphenylamines and dibenzothiophene sulfones, and Pd and their control materials (AG–Pd, MOP–TADS–Pd2).

building blocks (Fig. S2 in the ESI†). In addition, another control material, MOP–TADS–Pd2, was prepared under the same synthetic conditions as AG–MOP–TADS–Pd2 without using AG.

Scanning electron microscopy (SEM) showed that commercial AG is made up of 10–50 micron sized particles with relatively smooth surface (Fig. 3a and b). In comparison, granular MOP–TADS–Pds were loaded on the surface of AG in the AG–MOP–TADS–Pds (Fig. 3c–f). Energy dispersive X-ray spectroscopy (EDS)-based elemental mapping analysis showed the homogeneous distribution of Sr, Al, O, C, N, S, and Pd over AG–MOP–TADS–Pd2, indicating the loading of MOP–TADS and Pd on the AG (Fig. 3g). Transmission electron microscopy (TEM) and high resolution TEM analysis showed the incorporation of Pd nanoparticles with a diameter of 5–7 nm into MOP–TADS (Fig. S3 in the ESI†).

 This journal is © The Royal Society of Chemistry 2023

Published on 12 Motsheanong 2023. Downloaded on 2025-09-05 03:40:57.

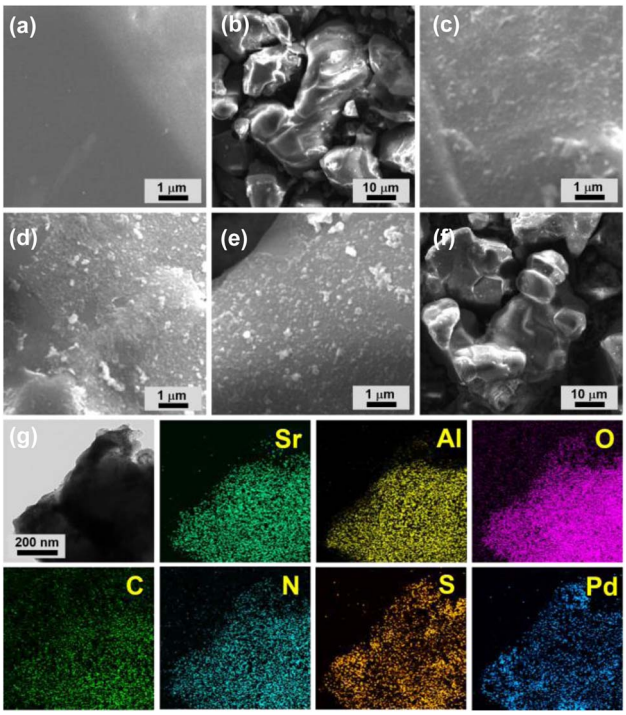

Fig. 3 SEM images of (a and b) AG, (c) AG–MOP–TADS–Pd1, (d and f) AG–MOP–TADS–Pd2, and (e) AG–MOP–TADS–Pd3. (g) EDS-based elemental mapping images of AG–MOP–TADS–Pd2.

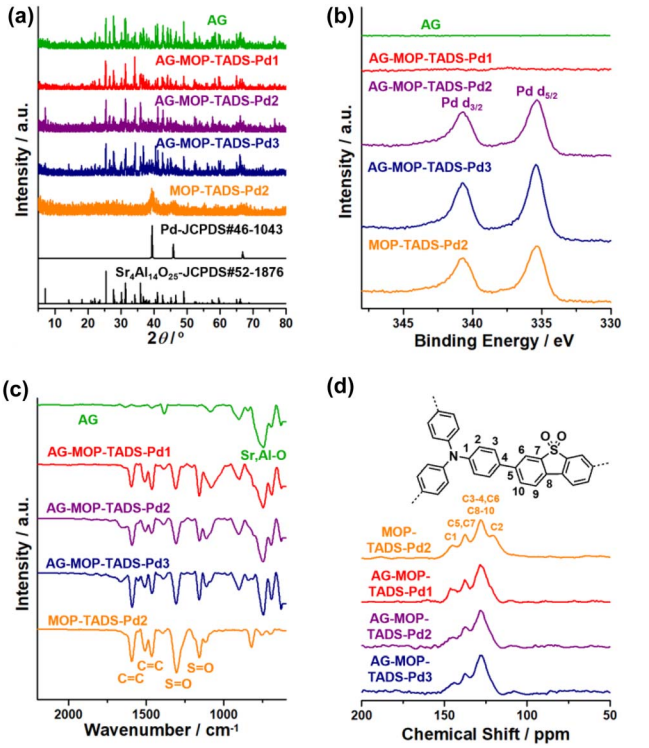

Fig. 4 (a) PXRD patterns, (b) XPS, and (c) IR spectra of AG, AG–MOP–TADS–Pds, and MOP–TADS–Pd2, and (d) solid state ^{13}C NMR spectra of AG–MOP–TADS–Pds and MOP–TADS–Pd2.

Powder X-ray diffraction (PXRD) studies showed that AG has a crystalline structure of $Sr_4Al_{14}O_{25}$ (JCPDS # 52-1876) (Fig. 4a). The PXRD pattern of MOP–TADS–Pd2 showed the diffraction peaks of zerovalent Pd (JCPDS # 46-1043). In the cases of AG–MOP–TADS–Pds, while the diffraction peaks of AG were mainly observed, those of zerovalent Pd gradually increased with increasing Pd amounts from AG–MOP–TADS–Pd1 to AG–MOP–TADS–Pd2 and AG–MOP–TADS–Pd3, respectively. The MOP–TADS obtained by Pd etching from MOP–TADS–Pd2 was amorphous, matching with the conventional properties of MOPs in the literature (Fig. S4 in the ESI†).[9]

The X-ray photoelectron spectra (XPS) of AG–MOP–TADS–Pd2, AG–MOP–TADS–Pd3, and MOP–TADS–Pd2 showed Pd 3d orbital peaks at 340.7 and 335.4 eV, corresponding to the zerovalent Pd species (Fig. 4b and S5 in the ESI†).[16] In comparison, the XPS spectrum of AG–MOP–TADS–Pd1 revealed trace Pd 3d orbital peaks, due to the minor amount of Pd in the materials.

The N_2 sorption studies based on Brunauer–Emmett–Teller theory showed that MOP–TADS has a surface area of 249 $m^2\ g^{-1}$ and microporosity (Fig. S6 in the ESI†). The chemical structures of the materials were characterized by infrared absorption (IR) and solid state ^{13}C nuclear magnetic resonance (NMR) spectroscopy (Fig. 4c and d). While AG showed Sr–O or Al–O vibration peaks at 747 cm^{-1},[18] the IR spectrum of MOP–TADS–Pd2 showed aromatic C=C vibration peaks at 1590 and 1465 cm^{-1} in addition to S=O vibrations of the sulfone groups at 1303 and 1159 cm^{-1}, matching with the expected chemical structures (Fig. 4c).[16] The solid state ^{13}C NMR spectrum of MOP–TADS–Pd2 showed aromatic ^{13}C peaks at 145, 137, 128, and 120 ppm, corresponding to aromatic carbons adjacent to nitrogens, dibenzothiophene sulfones, overlapped aromatic carbons, and triphenylamines, respectively (Fig. 4d).[16] The ^{13}C NMR spectra of AG–MOP–TADS–Pds showed the same ^{13}C peaks as MOP–TADS–Pd2, indicating that the MOP–TADS of AG–MOP–TADS–Pds has the same chemical structure as MOP–TADS–Pd2. Based on thermogravimetric analysis (TGA) and inductively coupled plasma atomic emission spectroscopy (ICP-AES), the content of MOP–TADS–Pds in the AG–MOP–TADS–Pd1, AG–MOP–TADS–Pd2, and AG–MOP–TADS–Pd3 was determined to be 5.9, 10.4, and 13.3 wt%, respectively.

The optical properties of AG, AG–MOP–TADS–Pds, and MOP–TADS–Pd2 were investigated by reflectance and emission spectroscopy (Fig. 5). While AG had a white ivory appearance, AG–MOP–TADS–Pd1 turned yellow (Fig. 5a and c). With increasing amounts of Pd, the colors of MOP–TADS–Pd2, AG–MOP–TADS–Pd2, and AG–MOP–TADS–Pd3 became darker (Fig. 5b, d and e). The aqueous suspension of AG–MOP–TADS–Pd2 showed bright emission after light irradiation (Fig. 5f). The absorption behaviors of the materials were investigated through the conversion of reflectance spectra (Fig. 5g). Whilst AG showed absorption at 340–474 nm, MOP–TADS–Pd2 showed two absorption bands at 340–535 nm and 535–800 nm, corresponding to the absorption by MOP–TADS and black Pd nanoparticles, respectively. While AG–MOP–TADS–Pds showed the same absorption of MOP–TADS at 340–535 nm, the absorption at 535–800 nm gradually increased with increasing amounts of Pd. In emission spectroscopy, AG showed strong emission at

Published on 12 Motsheanong 2023. Downloaded on 2025-09-05 03:40:57.

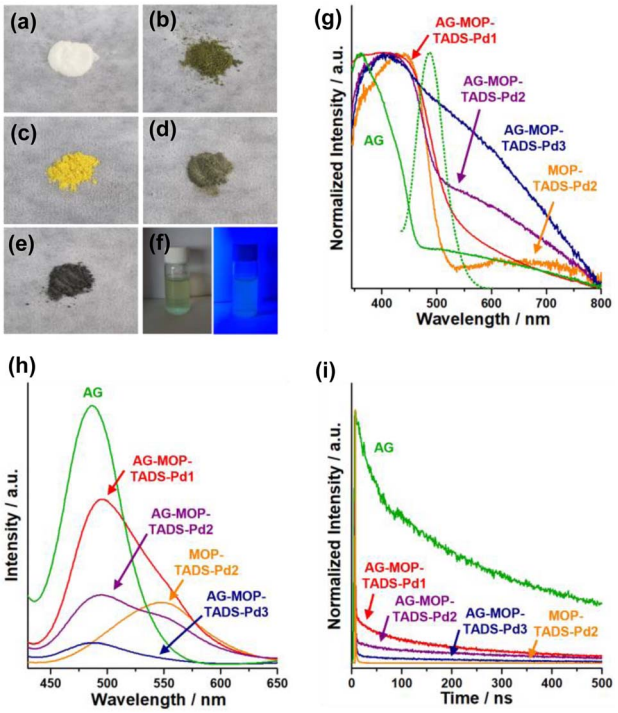

Fig. 5 Photographs of (a) AG, (b) MOP–TADS–Pd2, (c) AG–MOP–TADS–Pd1, (d) AG–MOP–TADS–Pd2, (e) AG–MOP–TADS–Pd3, and (f) an aqueous suspension of AG–MOP–TADS–Pd2 before and after light irradiation. (g) Absorption and (h) emission spectra (λ_{ex} 360 nm) and (i) emission decay curves of AG, AG–MOP–TADS–Pds, and MOP–TADS–Pd2. The emission of AG is indicated by a dotted line in (g).

400–595 nm, which overlapped with the absorption band of MOP–TADS–Pd2 in the range of 400–535 nm, indicating that the emission of AG can be absorbed by MOP–TADS *via* Förster resonance energy transfer (Fig. 5g and h).[19]

While MOP–TADS–Pd2 showed emission at 450–650 nm, the AG–MOP–TADS–Pds showed two emission bands at 400–595 nm and 450–650 nm by AG and MOP–TADS, respectively (Fig. 5h). With increasing amounts of MOP–TADS–Pd in AG–MOP–TADS–Pds, the emission intensities gradually decreased, indicating efficient charge transfer between AG, MOP–TADS, and Pd. The emission decay behaviors were investigated by laser photophysical studies (Fig. 5i). While the emission by AG showed a long average lifetime of 360 ns, the average emission lifetime of AG–MOP–TADS–Pds gradually decreased to 36, 23, and 8 ns for AG–MOP–TADS–Pd1, AG–MOP–TADS–Pd2, and AG–MOP–TADS–Pd3, respectively (Fig. 5i and S7 in the ESI†). It is noteworthy that the emission of AG–Pd retained a long average lifetime of 362 ns, indicating that the reduced emission lifetimes of AG–MOP–TADS–Pds are attributable to the charge transfer between AG and MOP–TADS.

Next, the photocatalytic performance of the materials for hydrogen evolution from water was investigated (Fig. 6). While AG was inactive in the photocatalytic hydrogen generation, the photocatalytic activity of AG–MOP–TADS–Pd1 was relatively poor, due to the insufficient amount of Pd (0.05 wt%) (Fig. S1 in the ESI†). In comparison, while AG–MOP–TADS–Pd2 (6.3 wt%

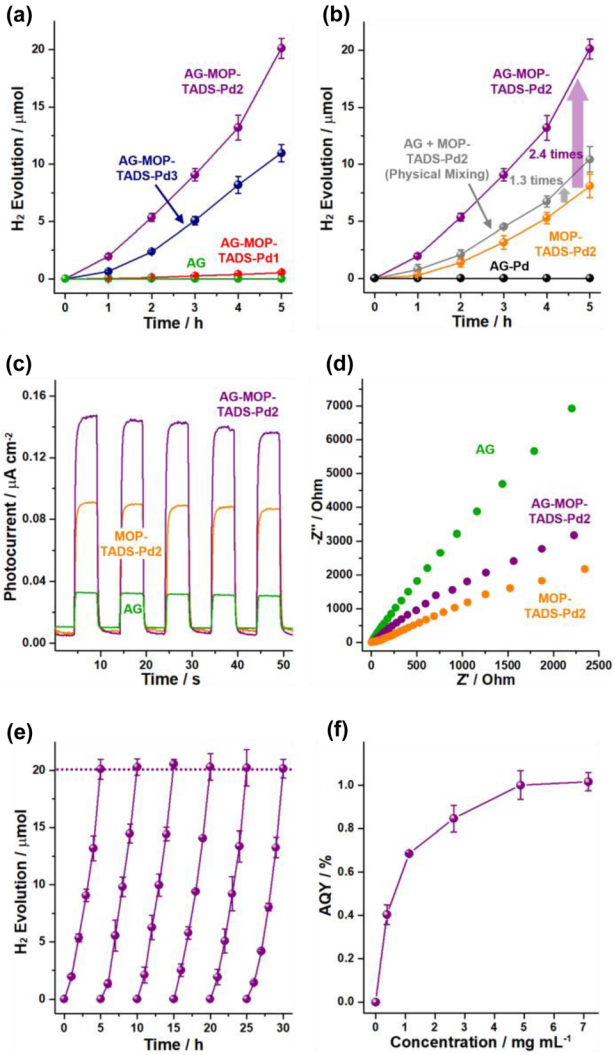

Fig. 6 (a and b) Photocatalytic hydrogen evolution (average values of five sets) by AG, AG–MOP–TADS–Pds, MOP–TADS–Pd2, a mixture of AG and MOP–TADS–Pd2, and AG–Pd (300 W Xe lamp, 10 v/v% TEOA as an electron sacrificer). (c) Photoelectrochemical studies and (d) Nyquist plots of AG–MOP–TADS–Pd2, MOP–TADS–Pd2, and AG. (e) Cycling tests and (f) AQYs (@420 nm) of photocatalytic hydrogen evolution by AG–MOP–TADS–Pd2.

Pd) showed promising photocatalytic performance, the hydrogen evolution activity of AG–MOP–TADS–Pd3 (9.7 wt% Pd) decreased, compared with that of AG–MOP–TADS–Pd2, indicating that the AG–MOP–TADS–Pd2 is an optimal material (Fig. 6a). It has been well recognized that the optimal amount of Pd is critical to achieving efficient performance of MOP-based photocatalysts (Fig. S1 in the ESI†).[16] In control studies, AG–Pd (5.6 wt% Pd) that had been prepared under the same synthetic conditions as AG–MOP–TADS–Pd2 in the absence of organic building blocks showed no hydrogen production (Fig. 6b and refer to the Experimental section in the ESI† for detailed procedures), revealing that the photocatalytic hydrogen evolution resulted from MOP–TADS–Pds. The introduction of AG into AG–MOP–TADS–Pd2 (6.3 wt% Pd) significantly enhanced hydrogen production by 2.4 times, compared with

 This journal is © The Royal Society of Chemistry 2023

Published on 12 Motsheanong 2023. Downloaded on 2025-09-05 03:40:57.

MOP–TADS–Pd2 (6.1 wt% Pd) (indicated by a violet arrow in Fig. 6b).

While the hydrogen evolution rate (HER) of MOP–TADS–Pd2 is 5.27×10^3 μmol g^{-1} h^{-1}, that of MOP–TADS–Pd in AG–MOP–TADS–Pd2 corresponds to 1.29×10^4 μmol g^{-1} h^{-1}, indicating that the AG plays a positive role including in the possible scattering effect[12b] in the photocatalytic production of hydrogen. It is noteworthy that during 2014–2020, MOP-based photocatalysts had shown HERs in the range of 1×10^2 to 8.52×10^3 μmol g^{-1} h^{-1} in the literature (Table S1 in the ESI†).[5–8] In the last two years, the HERs of MOP-based photocatalysts have been improved up to 1.58×10^5 μmol g^{-1} h^{-1} in the literature.[5–8] Although the HER performance of this work is not at the level of the world's best records, it reflects the significant improvement of the MOP-based photocatalysts developed by our research group[10,15] from 1.25×10^3 μmol g^{-1} h^{-1} to 1.29×10^4 μmol g^{-1} h^{-1} (Table S1 in the ESI†). When we physically mixed the AG with MOP–TADS–Pd2, the HER increased by 1.3 times, compared with that of MOP–TADS–Pd2, indicating that the contact of MOP–TADS–Pd2 on the AG is also important for efficient hydrogen production (Fig. 6b and S1 in the ESI†).

To rationalize the superior photocatalytic performance of AG–MOP–TADS–Pd2, photoelectrochemical studies were conducted. As displayed in Fig. 6c, AG–MOP–TADS–Pd2 showed an enhanced photocurrent response, compared with AG and MOP–TADS–Pd2, indicating synergistic action between AG and MOP–TADS–Pd2 for efficient photo-induced charge transfer. Electrochemical impedance spectroscopy (EIS) showed that as the amount of AG increased from MOP–TADS–Pd2 to AG–MOP–TADS–Pd2 and AG, charge transfer resistances increased (Fig. 6d). These results imply that AG assisted the photocatalytic performance of AG–MOP–TADS–Pd2 in a photoelectrochemical manner.

Cycling tests of photocatalytic hydrogen evolution by AG–MOP–TADS–Pd2 were conducted (Fig. 6e). For 5 additional cycling tests, the photocatalytic hydrogen evolution rates remained in the range of 100–102%. IR and XPS studies showed that the AG–MOP–TADS–Pd2 recovered after 5 additional cycles completely retained the original chemical structure (Fig. S8 in the ESI†). Apparent quantum yields (AQYs) were measured at 420 nm by changing the concentration of AG–MOP–TADS–Pd2 (Fig. 6f), showing that the maximum AQY reached 1.02%. While higher AQYs (@420 nm) of the MOP-based photocatalysts for hydrogen evolution have been recently reported,[8] it is noteworthy that the representative conjugated microporous polymer-based photocatalytic systems prepared by Cooper's research group showed AQYs (@420 nm) of 0.23% and 0.42% (Table S1 in the ESI†).[6]

The photocatalytic process of AG–MOP–TADS–Pd2 was further rationalized with a density functional theory (DFT)-based computational simulation (Fig. 7 and S9–S12 in the ESI†). First, the ground state ionization energy (IP) and the excited state ionization energy (IP*) of MOP–TADS were computed to be 0.64–0.70 eV and −1.85 to −1.89 eV (*vs.* NHE), respectively, through the gradual extension of model systems (Fig. 7a and b). Second, to calculate the energy levels of AG,

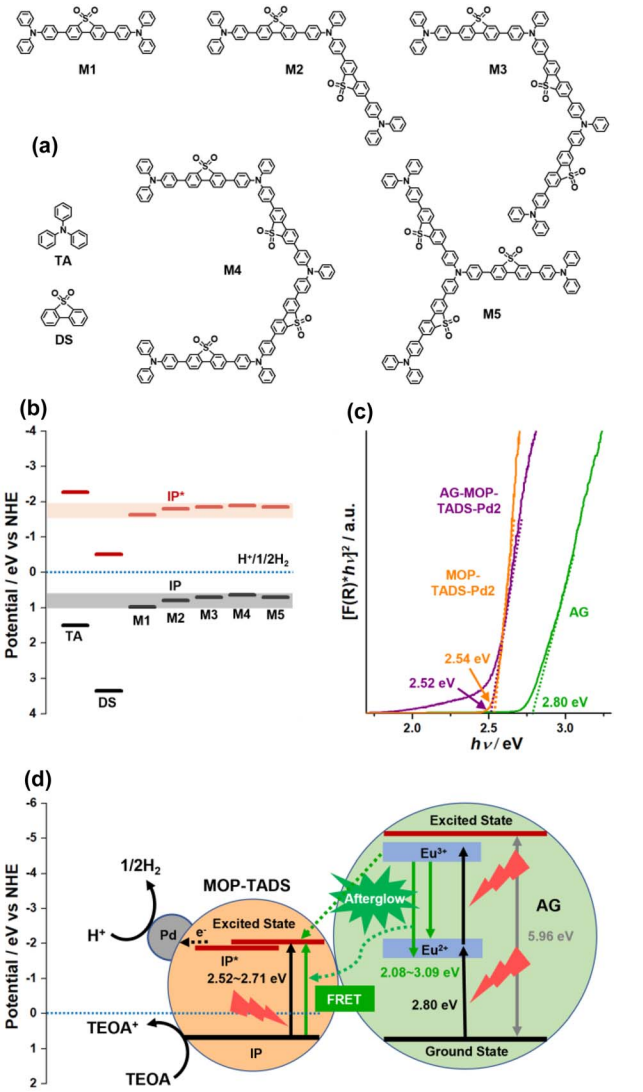

Fig. 7 (a) The model systems of MOP–TADS for DFT-based computational studies. (b) The simulated IP and IP* energy levels of the model systems of MOP–TADS. (c) The Kubelka–Munk plots of the reflectance spectra of AG, AG–MOP–TADS–Pd2, and MOP–TADS–Pd2. (d) The suggested photocatalytic hydrogen evolution process of AG–MOP–TADS–Pd2 based on DFT calculation and experimental optical results. IP and IP* refer to the calculated ground state ionization potential and excited state ionization potential, respectively. FRET in (d) stands for Förster resonance energy transfer.

a bulk unit cell and the surface slab model of $Sr_4Al_{14}O_{25}$ with a *Pmma* space group were optimized at PBE/light tier-1 level (Fig. S9–S12 in the ESI†). Then, the IP and the band gap of AG were simulated to be 0.74 (*vs.* NHE) and 5.96 eV, respectively. The Kubelka–Munk plots of the reflectance spectra indicated the band gaps of AG, MOP–TADS–Pd2, and AG–MOP–TADS–Pd2 to be 2.80, 2.54, and 2.52 eV, respectively (Fig. 7c). According to emission spectroscopy, the emission range of AG was 2.08–3.09 eV. Thus, as shown in Fig. 7d, it can be speculated that the afterglow emission of AG can induce the FRET from AG to MOP–TADS–Pd (2.52–2.71 eV) in the AG–MOP–TADS–Pd2 (indicated by a dotted curved arrow). In addition, charge transfer between

Published on 12 Motsheanong 2023. Downloaded on 2025-09-05 03:40:57.

the excited state of AG and MOP–TADS can occur (indicated by a dotted straight arrow in Fig. 7d). Finally, electrons can be transferred from the excited state of MOP–TADS to Pd nanoparticles to reduce protons to hydrogen gas, in addition to the oxidation of triethanolamine.

In conclusion, this work presents a conceptual approach for enhancing the hydrogen production efficiency of MOP-based photocatalysts by incorporating AG materials. The incorporation of MOP-based photocatalysts on the surface of AG resulted in enhanced hydrogen evolution efficiency by 2.4 times, compared with the control MOP-based photocatalysts, due to the efficient light utilization with the help of AG. We believe that the photocatalytic performance of AG–MOP materials can be further improved by applying nano-sized AGs instead of micron-sized ones.

Author contributions

S. U. Son: conceptualization, supervision, writing the original draft, and review & editing. K. C. Ko and T. K. Ahn: supervision and review. S. H. Ryu and G. H. Kim: investigation and formal analysis.

Conflicts of interest

There are no conflicts to declare.

Acknowledgements

This work was supported by National Research Foundation of Korea (NRF) grants (no. RS-2023-00208797 and NRF-2020R1F1A1076128) funded by the Korean government (MSIT).

Notes and references

1 Z. Liu, Z. Deng, S. J. Davis, C. Giron and P. Ciais, *Nat. Rev. Earth Environ.*, 2022, **3**, 217–219C.

2 M. Yue, H. Lambert, E. Pahon, R. Roche, S. Jemei and D. Hissel, *Renewable Sustainable Energy Rev.*, 2021, **146**, 111180.

3 P. J. Megía, A. J. Vizcaíno, J. A. Calles and A. Carrero, *Energy Fuels*, 2021, **35**, 16403–16415.

4 (*a*) X. Tao, Y. Zhao, S. Wang, C. Li and R. Li, *Chem. Soc. Rev.*, 2022, **51**, 3561–3608; (*b*) Q. Wang and K. Domen, *Chem. Rev.*, 2020, **120**, 919–985.

5 (*a*) Y. Wang, A. Vogel, M. Sachs, R. S. Sprick, L. Wilbraham, S. J. A. Moniz, R. Godin, M. A. Zwijnenburg, J. R. Durrant, A. I. Copper and J. Tang, *Nat. Energy*, 2019, **4**, 746–760; (*b*) Y. Bai, K. Hippalgaonkar and R. S. Sprick, *J. Mater. Chem. A*, 2021, **9**, 16222–16232; (*c*) Y. Liu, B. Li and Z. Xiang, *Small*, 2021, **17**, 2007576.

6 (*a*) R. S. Sprick, J.-X. Jiang, B. Bonillo, S. Ren, T. Ratvijitvech, P. Guiglion, M. A. Zwijnenburg, D. J. Adams and A. I. Copper, *J. Am. Chem. Soc.*, 2015, **137**, 3265–3270; (*b*) R. S. Sprick, B. Bonillo, M. Sachs, R. Clowes, J. R. Durrant, D. J. Adams and A. I. Cooper, *Chem. Commun.*, 2016, **52**, 10008–10011.

7 (*a*) M. G. Schwab, M. Hamburger, X. Feng, J. Shu, H. W. Spiess, X. Wang, M. Antonietti and K. Müllen, *Chem. Commun.*, 2010, **46**, 8932–8934; (*b*) C. Yang, B. C. Ma, L. Zhang, S. Lin, S. Ghasimi, K. Landfester, K. A. I. Zhang and X. Wang, *Angew. Chem., Int. Ed.*, 2016, **55**, 9202–9206; (*c*) L. Li and Z. Cai, *Polym. Chem.*, 2016, **7**, 4937–4943; (*d*) L. Wang, Y. Wan, Y. Ding, S. Wu, Y. Zhang, X. Zhang, G. Zhang, Y. Xiong, X. Wu, J. Yang and H. Xu, *Adv. Mater.*, 2017, **29**, 1702428; (*e*) Y. Xu, N. Mao, S. Feng, C. Zhang, F. Wang, Y. Chen, J. Zeng and J.-X. Jiang, *Macromol. Chem. Phys.*, 2017, **218**, 1700049; (*f*) Y. Xu, C. Zhang, P. Mu, N. Mao, X. Wang, Q. He, F. Wang and J.-X. Jiang, *Sci. China: Chem.*, 2017, **60**, 1075–1083; (*g*) L. Wang, X. Zheng, L. Chen, Y. Xiong and H. Xu, *Angew. Chem., Int. Ed.*, 2018, **57**, 3454–3458; (*h*) Y. Zhao, W. Ma, Y. Xu, C. Zhang, Q. Wang, T. Yang, X. Gao, F. Wang, C. Yan and J.-X. Jiang, *Macromolecules*, 2018, **51**, 9502–9508; (*i*) Z. Wang, X. Yang, T. Yang, Y. Zhao, F. Wang, Y. Chen, J. H. Zeng, C. Yan, F. Huang and J.-X. Jiang, *ACS Catal.*, 2018, **8**, 8590–8596; (*j*) R. S. Sprick, Y. Bai, A. A. Y. Guibert, M. Zbiri, C. M. Aitchison, L. Wilbraham, Y. Yan, D. J. Woods, M. A. Zwijnenburg and A. I. Cooper, *Chem. Mater.*, 2019, **31**, 305–313; (*k*) X.-J. Xiao, Y. Wang, W.-R. Wang, J. Li, J. Wang, Z.-W. Xu, J. Li, J. Yao and W.-S. Li, *Macromolecules*, 2020, **53**, 2454–5463.

8 (*a*) J.-L. Wang, G. Ouyang, D. Wang, J. Li, J. Yao, W.-S. Li and H. Li, *Macromolecules*, 2021, **54**, 2661–2664; (*b*) C. Shu, C. Han, X. Yang, C. Zhang, Y. Chen, S. Ren, F. Wang, F. Huang and J.-X. Jiang, *Adv. Mater.*, 2021, **33**, 2008498; (*c*) M. G. Mohamed, M. H. Elsayed, A. M. Elewa, A. F. M. EL-Mahdy, C.-H. Yang, A. A. K. Mohammed, H.-H. Chou and S.-W. Kuo, *Catal. Sci. Technol.*, 2021, **11**, 2229–2241; (*d*) C. Han, P. Dong, H. Tang, P. Zheng, C. Zhang, F. Wang, F. Huang and J.-X. Jiang, *Chem. Sci.*, 2021, **12**, 1796–1802; (*e*) X. Zhao, B. Chen, W. Dong, S. Wang, Y. Xiang and H. Chen, *J. Mater. Chem. A*, 2021, **9**, 10208–10216; (*f*) C. Yang, Z. Cheng, G. Divitini, C. Qian, B. Hou and Y. Liao, *J. Mater. Chem. A*, 2021, **9**, 19894–19900; (*g*) C. Han, S. Xiang, M. Ge, P. Xie, C. Zhang and J.-X. Jiang, *Small*, 2022, **18**, 2202072; (*h*) Z.-R. Tang, Y.-Q. Xing, J.-Z. Cheng, G. Zhang, Z.-Q. Shen, Y.-J. Zhang, G. Liao, L. Chen and S.-Y. Liu, *Chem. Sci.*, 2022, **13**, 1725–1733; (*i*) X. Han, Y. Zhang, Y. Dong, J. Zhao, S. Ming and J. Zhang, *RSC Adv.*, 2022, **12**, 708–718; (*j*) C. Han, S. Xiang, P. Xie, P. Dong, C. Shu, C. Zhang and J.-X. Jiang, *Adv. Funct. Mater.*, 2022, **32**, 2109423; (*k*) H. Zhao, Y. Dong, P. Sun, Y. Bai, C. Ru, X. Wu, Z. Li, X. Han, J. Wu and X. Pan, *ACS Appl. Energy Mater.*, 2022, **5**, 4631–4640; (*l*) R. Li, C. Zhang, C.-X. Cui, Y. Hou, H. Niu, C.-H. Tan, X. Yang, F. Huang, J.-X. Jiang and Y. Zhang, *Polymer*, 2022, **240**, 124509.

9 (*a*) M. G. Mohamed, A. F. M. El-Mahdy, M. G. Kotp and S.-W. Kuo, *Mater. Adv.*, 2022, **3**, 707–733; (*b*) J.-S. M. Lee and A. I. Cooper, *Chem. Rev.*, 2020, **120**, 2171–2214; (*c*) D. Taylor, S. J. Dalgarno, Z. Xu and F. Vilela, *Chem. Soc. Rev.*, 2020, **49**, 3981–4042; (*d*) J. Wu, F. Xu, S. Li, P. Ma, X. Zhang, Q. Liu, R. Fu and D. Wu, *Adv. Mater.*, 2019, **31**, 1802922; (*e*) B. Zheng, X. Lin, X. Zhang, D. Wu and

 This journal is © The Royal Society of Chemistry 2023

Published on 12 Motsheanong 2023. Downloaded on 2025-09-05 03:40:57.

K. Matyjaszewski, *Adv. Funct. Mater.*, 2019, 1907006; (*f*) N. Chaoui, M. Trunk, R. Dawson, J. Schmidt and A. Thomas, *Chem. Soc. Rev.*, 2017, **46**, 3302–3321; (*g*) L. Tan and B. Tan, *Chem. Soc. Rev.*, 2017, **46**, 3322–3356; (*h*) S. Das, P. Heasman, T. Ben and S. Qiu, *Chem. Rev.*, 2017, **117**, 1515–1563; (*i*) J.-K. Sun, M. Antonietti and J. Yuan, *Chem. Soc. Rev.*, 2016, **45**, 6627–6656; (*j*) Y. Xu, S. Jin, H. Xu, A. Nagai and D. Jiang, *Chem. Soc. Rev.*, 2013, **42**, 8012–8031; (*k*) D. Wu, F. Xu, B. Sun, R. Fu, H. He and K. Matyjaszewski, *Chem. Rev.*, 2012, **112**, 3959–4015.

10 J. H. Park, K. C. Ko, N. Park, H.-W. Shin, E. Kim, N. Kang, J. H. Ko, S. M. Lee, H. J. Kim, T. K. Ahn, J. Y. Lee and S. U. Son, *J. Mater. Chem. A*, 2014, **2**, 7656–7661.

11 L. Li, Z. Cai, Q. Wu, W.-Y. Lo, N. Zhang, L. X. Chen and L. Yu, *J. Am. Chem. Soc.*, 2016, **138**, 7681–7686.

12 (*a*) X. Liu, X. Chen, Y. Li, B. Wu, X. Luo, S. Quyang, S. Luo, A. A. A. Kheraif and J. Lin, *J. Mater. Chem. A*, 2019, **7**, 19173–19186; (*b*) M. N. Mustafa, S. Shafie, M. H. Wahid and Y. Sulaiman, *Sci. Rep.*, 2019, **9**, 14952; (*c*) F. Berry, R. Mermet-Lyaudoz, J. M. C. Davila, D. A. Djemmah, H. S. Nguyen, C. Seassal, E. Fourmond, C. Chevalier, M. Amara and E. Drouard, *Adv. Energy Mater.*, 2022, **12**, 2200505.

13 D. V. Heggen, J. J. Joos, A. Feng, V. Fritz, T. Delgado, N. Gartmann, B. Walfort, D. Rytz, H. Hagemann, D. Poelman, B. Viana and P. F. Smet, *Adv. Funct. Mater.*, 2022, 2208809.

14 (*a*) T. Matsuzawa, Y. Aoki, N. Takeuchi and Y. Murayama, *J. Electrochem. Soc.*, 1996, **143**, 2670–2673; (*b*) C. Chang, Z. Yuan and D. Mao, *J. Alloys Compd.*, 2006, **415**, 220–224; (*c*) D. Dutczak, T. Justel, C. Ronda and A. Meijerink, *Phys. Chem. Chem. Phys.*, 2015, **17**, 15236–15249.

15 K. Cho, C. W. Kang, S. H. Ryu, J. Y. Jang and S. U. Son, *J. Mater. Chem. A*, 2022, **10**, 6950–6954.

16 S. H. Ryu, S. M. Lee, H. J. Kim, Y.-J. Ko, K. C. Ko and S. U. Son, *J. Mater. Chem. A*, 2021, **9**, 22262–22268.

17 (*a*) N. Kang, J. H. Park, M. Jin, N. Park, S. M. Lee, H. J. Kim, J. M. Kim and S. U. Son, *J. Am. Chem. Soc.*, 2013, **135**, 19115–19118; (*b*) C. W. Kang, D.-M. Lee, J. Park, S. Bang, S.-W. Kim and S. U. Son, *Angew. Chem., Int. Ed.*, 2022, **61**, 2202209659.

18 F. Li, Z. Li, X. Wang, M. Zhang, Y. Shen, P. Cai and X. He, *J. Alloys Compd.*, 2017, **695**, 10–21.

19 (*a*) T. Förster, *Ann. Phys.*, 1948, **2**, 55–75; (*b*) A. Kaur, P. Kaur and S. Ahuja, *Anal. Methods*, 2020, **12**, 5532–5550.